# HETEROPOLYNUCLEAR Pt(II)-M(I) CLUSTERS WITH A C^N^C BIS-CYCLOMETALATED LIGAND

*Sara Fuertes,[a] Christopher H. Woodall,[a] Paul. R. Raithby,*[a] and Violeta Sicilia*[b]*

[a]Department of Chemistry, University of Bath, Bath, BA2 7AY (United Kingdom). E-mail: p.r.raithby@bath.ac.uk. Fax: (+44) 1225 383183.

[b]Instituto de Síntesis Química y Catálisis Homogénea (ISQCH), CSIC - Universidad de Zaragoza, Departamento de Química Inorgánica, Escuela de Ingeniería y Arquitectura de Zaragoza, Campus Río Ebro, Edificio Torres Quevedo, 50018, Zaragoza (Spain). E-mail: sicilia@unizar.es

**RECEIVED DATE (to be automatically inserted after your manuscript is accepted if required according to the journal that you are submitting your paper to)**

**Abstract**

The mononuclear complex [($EtO_2C$-C^N^C)Pt(dmpyz)] (**1**) (dmpyz = 2,5-dimethylpyrazine) has been synthesised by reaction of [($EtO_2C$-C^N^C)Pt(dmso)] (**A**) with dmpyz in 1:1 molar ratio in dichloromethane. Complex **1** is the precursor for preparing the homodinuclear complex [{($EtO_2C$-C^N^C)Pt}$_2$($\mu$-dmpyz)] (**2**) and the heterotrinuclear clusters [{($EtO_2C$-C^N^C)Pt(dmpyz)}$_2$M]X (M= Cu, X= $PF_6$ (**3**); M= Ag, X= $BF_4$ (**4**)). Compounds **1**, **2** and **4** were studied by X-ray diffraction methods. In the crystal packing of **1** and **2**, the molecules display short intermolecular π···π contacts, which control the solid state emissive behavior. X-ray study on **4** shows two [$Pt_2Ag$] sandwich-type clusters in the asymmetric unit, both with the two square–planar "(R-CNC)Pt(dmpyz)" moieties stabilized by two Pt→Ag donor-acceptor bonds as well as by $\eta^1$- and $\eta^2$-Ag-C interactions. Intramolecular π-π contacts were found between the pyridine rings of the CNC ligands within the same $Pt_2Ag$ cluster. $^1$H and $^{195}$Pt NMR studies confirm that the $Pt_2M$ cluster is also retained in solution at room temperature. $^{195}$Pt NMR spectra of **3** and **4** show signals shifted significantly downfield when comparing to that for the monomer (**1**), which is attributed to presence of Pt-M dative bonds. At lower temperatures (T = 193 K), the copper derivative definitely falls apart, whereas the silver one still holds up unbroken. In solid state at 77 K, compounds **1**-**4** give red emissions arising from $^3$ππ excited states due to the intra- or intermolecular π-π contacts observed in the crystal structures. As expected, in glassy solutions (77 K), compound **3** displays analogous emissions to those from the starting material (**1**). Complexes **1** and **2** show structured emission bands which are particularly sensitive to the λex (HE and LE). In contrast, **4** displays an unstructured emission at 680 nm with a shoulder at 556 nm, both are not dependent on the λex. DFT and TDDFT computational studies have been performed on **1** and **2** which support the conclusions drawn from the photophysical studies.

## Introduction

Metallophilic interactions between closed or pseudo closed shell transition metals have attracted considerable interest because of their versatile applications in the field of metal cluster chemistry,[1-4] catalysis,[5,6] crystal engineering[7-9] and luminescent materials.[10-12] Square-planar platinum (II) complexes are well-known to form heteropolynuclear clusters containing metal-metal interactions ($d^{8\cdots}$ $d^{10}$, $d^{8\cdots}s^2$) [M = Cu(I),[10-15] Ag(I),[10-12,15-18] Au(I),[10,15,19,20] Pb(II),[21-24] Cd(II), [25-27] Tl(I)[28-31]] that display remarkable structural and photophysical properties.[32]

The Pt→M dative bond is a particular type of metal–metal interaction which takes place between an electron rich platinum center and a Lewis acidic metal. The molecular orbitals scheme for this Pt→M donor acceptor bond indicates that the stronger dative bond will be formed as the platinum $d_z^2$ orbital is raised in energy, which will be likely to occur when the platinum center is placed in a strong ligand field.[33,34] Therefore, square-planar cyclometalated complexes with π-conjugated ligands seem to be suitable systems due to the electronic features of the C-σ bond (σ donor) and the aromatic fragment (π acceptor). Platinum (II) complexes containing C^N-bidentate or C^N^N, N^C^N, C^N^C, C^N^S-tridentate chelating ligands have been investigated recently because of the potential use as anti-cancer agents,[35-40] imaging species for biomolecules[37,40-43] as well as for the development of new tuneable optoelectronic molecular devices,[44-49] dye-sensitized solar cells[50,51] and sensor manufacturing.[52,53] Most of these applications can be related to the outstanding photophysical behaviour of these complexes.[54,55] Their emissive properties normally rely on ligand centered (LC) or metal-to-ligand charge-transfers (MLCT) transitions, which are characteristic of the monomeric species. Since these complexes are not sterically hindered they can interact with each other through π···π or Pt···Pt interactions creating excimers or aggregates with a consequent change in the nature of the emissive state (ππ* or MMLCT).[49,56-62]

As mentioned above, a platinum center surrounded by a strong ligand field would favour the formation of Pt→M dative bonds; those electronic requirements can also be achieved by selecting the appropriate ancillary ligands. Therefore, it has been widely reported that homo- and heteroleptic electron rich platinum complexes using ligands such as cyanide,[21,28,31,63] alkynyl[15,16,27,29-31,64,65] and/or perhalophenyl[18,22,24,66,67] are likely to form polymetallic compounds with Pt(II)→M bonds.

So far, our research and that of other groups on platinum complexes containing chromophoric cyclometalated ligands has only identified a rather limited number of heteropolynuclear complexes with Pt(II)-Ag(I),[17,68-71] Pt(II)-Tl(I),[31,65] Pt(II)-Cd(II)[25,26] and Pt(II)-Pb(II)[23] donor-acceptor bonds. All these complexes were synthesised using very similar C^N bidentate ligands: 2-phenylpyridine, benzo{h}quinoline and 2-(2-thienyl)pyridine. To the best of our knowledge, there are no examples using tridentate chelating ligands or more concisely any bis-cycloplatinated ligand (C^N^C), which potentially could induced a stronger ligand field since it has two C-$\sigma$ bonds within the same ligand.[72]

In our research we have pulled all these themes together and focused on the study of heteropolynuclear bis-cycloplatinated complexes using a derivative of the 2,6-diphenylpyridine: the ethyl 2,6-diphenylisonicotinate ligand ($EtO_2C$-C^N^C-$H_2$). In this paper, we describe the preparation of the neutral mononuclear complex [($EtO_2C$-C^N^C)Pt(dmpyz)] (**1**) (dmpyz = 2,5-dimethylpyrazine), which has been used as a building block to prepare the homodinuclear derivative [{($EtO_2C$-C^N^C)Pt}$_2$($\mu$-dmpyz)] (**2**) and the heterotrinuclear clusters [{($EtO_2C$-C^N^C)Pt(dmpyz)}$_2$M]X (M= Cu, X= $PF_6$ (**3**); M= Ag, X= $BF_4$ (**4**)). Both heterotrinuclear compounds, **3** and **4**, are the first examples of $Pt_2M$ clusters displaying Pt$\rightarrow$M dative bonds with a tridentate C^N^C bis-cyclometalated ligand. Their photophysical behavior in solid state and glassy solution media have been examined and correlated to the X-ray structures and $^{195}$Pt NMR Variable-Temperature experiments. TD-DFT computational studies have also been performed on complexes **1** and **2**.

## Results and Discussions

**Synthesis and characterization of Mono- and Homodinuclear complexes: [($EtO_2C$-C^N^C)Pt(dmpyz)] (1) and [{($EtO_2C$-C^N^C)Pt}$_2$($\mu$-dmpyz)] (2).** Compounds **1** and **2** were prepared by reaction of the dmso derivative [($EtO_2C$-C^N^C)Pt(dmso)] (**A**)[73] with dmpyz in 1:1 and 1:0.5 molar ratio respectively (see Scheme 1). Both neutral compounds (**1** and **2**) were obtained as pure air-stable orange solids and were fully characterised (See Experimental Section). It was found that the reaction to form **2** was a very slow process, taking 4 days to go to completion. Therefore, an alternative route was attempted. A dichloromethane solution of **1** was gently heated (40° C, 24 h) with equimolecular amounts of **A** to afford compound **2**. As has been previously observed, the coordination of the first nitrogen atom of the 2,5-dimethylpyrazine ligand (dmpyz) to platinum seems to decrease the basicity of the second nitrogen atom.[74] This would explain the inertia observed in the formation of **2**.

Scheme 1

Well resolved $^1$H NMR spectra were observed for **1** and **2**, displaying the expected signals for the "Pt($EtO_2C$-C^N^C)" moiety.[73] The assignments were based on $^1$H-$^1$H and $^1$H-$^{13}$C correlations (see Scheme 2 and Experimental section). The monotopic dmpyz group in **1** gives two singlets in the low field region with the subsequent $^{195}$Pt satellites [$\delta$= 8.87, $^3J_{Pt\text{-}H}$ = 49 Hz ($H^d$), $\delta$= 8.58, $^4J_{Pt\text{-}H}$ = 15 Hz ($H^b$)] (Scheme 2) and in the upfield region, two singlets are observed at 2.6 and 2.5 ppm corresponding to the methyl groups. In complex **2**, the dmpyz group is acting as a bridging ligand between two symmetrical "Pt($EtO_2C$-C^N^C)" moieties, therefore the spectrum is simplified. Only two singlets at 9.1 and 2.7 ppm, that are relatively deshielded to those observed in **1** are displayed. Chemical shifts and coupling constant values of either the monotopic (**1**) or ditopic (**2**) dmpyz ligand are similar to those found in the literature.[74-76]

Scheme 2

The crystal structures of **1** and **2** have been determined by X-ray diffraction studies (Figures 1 and 2, Table 1). Both present similar structural details, the platinum (II) centers adopt the expected distorted square–planar geometry imposed by the tridentate C^N^C ligand, which is reflected on the angle between the *trans* aryl carbon atoms (C(11)-Pt(1)-C(21) = 162.9(3)° in

**1**; 162.4(3)° and 162.7(3)° in **2**). These features as well as the rest of bond parameters observed in the crystal structures are characteristic of C^N^C platinum (II) complexes.[59,60,73,77-81] The dimethylpyrazine molecules, N-coordinated to the platinum centers either mono- (**1**) or ditopically (**2**), exhibit Pt-N bond distances (2.018(6) Å in **1**; 2.016(5) Å and 2.004(5) Å in **2**) similar to those observed in related pyrazine derivatives.[59,74,75,80] The pyrazine rings are almost perpendicular to the Pt(C^N^C) moieties, with dihedral angles of 71.5° in **1** and 83.1° and 69.7° in **2**. The platinum coordination planes in **2** are not co-planar; they form a dihedral angle of 13.4°.

Figure 1, Figure 2

In complex **1**, the molecules stack in columns with the assistance of fairly short intermolecular π···π contacts (3.38 - 3.45 Å)[59,60,73,77,82,83] between the aromatic rings of the C^N^C ligand (cyan dashed line, Figure 1b). There are also rather weak C-H···O interactions along the *c*-axis (red dashed line, Figure 1b) between the oxygen atom of the ester group and the dmpyz (d (H---O) = 2.34 Å; d (C---O) = 3.26 Å)[60,73,77,84] generating a 2D zig-zag network. By contrast, the crystal packing of complex **2** shows head to tail molecular pairs (Figure 2b) with short π···π (3.26 - 3.40 Å, cyan dashed line) and C-H (dmpyz)···O (ester) contacts (C···O 2.937 Å, H···O 2.49 Å, red dashed line).

**Synthesis and characterization of Heterotrinuclear complexes:**

**$[\{(EtO_2C\text{-}C\text{^}N\text{^}C)Pt(dmpyz)\}_2M]^+$ (M= Cu (3) and Ag(4)).**

Reactions of [(EtO$_2$C-C^N^C)Pt(dmpyz)] (**1**) with [Cu(MeCN)$_4$]PF$_6$ and AgBF$_4$ in 1:0.5 molar ratio give the corresponding heterotrinuclear compounds [{(EtO$_2$C-C^N^C)Pt(dmpyz)}$_2$M]X (M= Cu, X= PF$_6$ (**3**); M= Ag, X= BF$_4$ (**4**)), (See Scheme 1 and Experimental Section). However, reactions of **1** with equimolar quantities of either [Ag(OTf)(PPh$_3$)] or [Ag(OTf)(tht)] led to a mixture of complexes arising from the exchange of ligands between platinum and silver centres, since species: [(EtO$_2$C-C^N^C)Pt(tht)],[73] [(EtO$_2$C-C^N^C)Pt(PPh$_3$)][73] and "Ag(dmpyz)" have been detected by NMR and mass spectrometry. Compounds **3** and **4** were obtained as pure orange-reddish solids and fully characterised. The trinuclear Pt$_2$M nature for these species was supported by $^1$H and $^{195}$Pt NMR spectroscopy, elemental analysis, mass spectrometry and structurally confirmed by the X-ray diffraction study on compound **4**. Mass spectrometric analysis of acetonitrile solutions of **3** and **4** showed peaks at m/z = 1272.2 and 1317.2 corresponding to the fragments [**3**-PF$_6$]$^+$

and [**4**-$BF_4$]$^+$, respectively. The experimental isotopic distribution patterns closely matched with the calculated for the proposed trinuclear species (Figures S1 and S2).

*$^1$H and $^{195}$Pt{$^1$H} NMR spectroscopy*

$^1$H NMR spectra of **3** and **4** showed identical profiles but were significantly different from that observed in **1**. Upon coordination of the metal centre ($M^I$), the resonance signals for $H^d$ (dmpyz) are displayed as broad singlets shifted upfield to 8.57 (**3**) and 8.20 (**4**) ppm whereas the $H^b$ are shifted downfield. Also, the $H^2$ (CNC) resonances show considerable reductions of the $^3J_{Pt\text{-}H}$ coupling constants from 32 Hz in **1** to 27.5 and 20 Hz in **3** and **4**, respectively (see Experimental Section), which supports the existence of the Pt-M bonds in solution.[14,70,85] The presence of Pt(II)→M(I) dative bonds in solution is also based on $^{195}$Pt{$^1$H} NMR data (Table 2, Figure 3). Compounds **3** and **4** show broad $^{195}$Pt resonances at -3330 and -3240 ppm in $CD_2Cl_2$ solutions at room temperature. Downfield shifts of 160 and 250 ppm are observed for **3** and **4**, when compared to $^{195}$Pt signal in **1** (-3490 ppm), which is in agreement with previous reported results.[25,68,69] However, at lower temperature (193 K) the $^{195}$Pt NMR spectra of **3** and **4**, in $CD_2Cl_2$, show rather different patterns. Compound **3**, displays two signals at -3500 and -3525 ppm with hardly any remaining signal at around -3350 ppm which is still present at 223 K (Figure 3). The resonance at -3525 ppm can undoubtedly be assigned to compound **1** (-3523 ppm, Table 2), but the one at -3500 ppm might be due to the formation of Pt-Cu subproducts. Compound **4** also exhibits a less intense singlet at -3525 ppm (**1**) but the main signal consists in a doublet at -3272 ppm because of the coupling to the spin active $^{107,109}$Ag nuclei with an average $^{195}$Pt-$^{107,109}$Ag coupling constant value of 455 Hz. This value is in line with the reported value for [$Pt_2Me_2$(bhq)$_2$($\mu$-dppy)$_2Ag_2$($\mu$-acetone)]($BF_4$)$_2$.[70] Due to the small difference between the magnetogyric ratios of the silver isotopes the individual coupling constants $^{195}$Pt-$^{107}$Ag and $^{195}$Pt-$^{109}$Ag were not able to be determined. [11,70]

Low temperature experiments were repeated for **3** and **4**, in acetone-$d^6$ solutions, and similar results were obtained. Meanwhile compound **3** gave one $^{195}$Pt signal at -3544 ppm most probably due to complex **1**, compound **4** only exhibited the expected doublet at -3300 ppm with a Pt-$^{107,109}$Ag coupling constant of 440 Hz. There is a general trend observed in all resonances, they all exhibit an upfield shift when cooling down and also when acetone-$d^6$ is used instead of $CD_2Cl_2$. Despite of this, the difference between the $^{195}$Pt resonances in **1** and **4** are about the same (~250 ppm). According to these results, the $Pt_2Cu$ core seems to be less strongly bound than the $Pt_2Ag$ one because of the lesser downfield shift observed at room temperature solution and mainly because it starts to decompose at low temperature solutions

(T < 223 K) no matter the nature of the solvent, whereas the $Pt_2Ag$ core is retained in either low or room temperature solutions and even when using coordinating solvents such as acetone.

*X-Ray Diffraction*

The X-ray study on a single crystal of **4** (Figure 4, Table 3) shed some light on the trinuclear structure arrangement. Compound **4** crystallizes in the noncentrosymmetric orthorhombic space group *P*b$2_1$a (non standard setting of n° 29, Pca$2_1$), contains, in the asymmetric unit, two molecular cations (**4A**, **4B**), having similar structural details. Both molecular cations consist in a trinuclear [$Pt_2Ag$] sandwich-type cluster with the two square–planar "(R-CNC)Pt(dmpyz)" moieties held together by a silver atom through two Pt→Ag bonds. The "(R-CNC)Pt(dmpyz)" fragments from both molecular cations (**4A** and **4B**) display bond lengths and angles comparable to those found in **1**.

Figure 4

The Pt coordination planes form dihedral angles of 10.1° (**4A**) and 13.0° (**4B**) with separations between the two Pt centres of 5.14 Å and 5.19 Å, respectively. In each cationic complex two different Pt-Ag distances are found, one clearly shorter than the other: Pt-Ag(1) = 2.773(11)Å Pt(1), 2.959(11)Å Pt(2) in **4A** and Pt-Ag(2) = 2.807(12)Å Pt(3), 2.909(12)Å Pt(4) in **4B**. All of them are at the upper end of the range found for Pt(II)→Ag(I) donor acceptor bonds.[17,66,68,69,71]

The Pt-Ag-Pt angles are considerably distorted from linearity, 127.4(4)° (**4A**) and 130.4(4)° (**4B**) and the Pt-Ag vectors are displaced from the perpendicular [36.5° and 43.9° in **4A**; 38.0° and 41.1° in **4B**], deviated towards the metalated carbon atoms of the CNC ligand. Two different $\eta^1$- and $\eta^2$-Ag-C interactions are observed within the same cationic complex. It is worth noting that in both $Pt_2Ag$ clusters, the shortest Pt-Ag bond correlates with the $\eta^1$–Ag-C interaction [2.317(11) Å in **4A** and 2.315(12) Å in **4B**], whereas the longest Pt-Ag one is linked to the $\eta^2$–Ag-C interaction [2.283(10) Å, 2.591(11) Å in **4A** and 2.299(13) Å, 2.655(12) Å in **4B**]. As shown above, the $\eta^2$–Ag-C interaction is asymmetric, displaying shorter bond lengths with the metalated carbon atoms. As commonly observed, the existence of Ag-$C_{ar}$ interactions do not affect the C-C distances in the aromatic ring. Similar structural features have been observed in related cyclometalated $Pt_2Ag$ clusters.[17,68,70,71,86]

It has been found in some related PtAg clusters that the silver centre tends to complete its coordination environment with solvent molecules.[68-71,87] By contrast in our case although the crystals were obtained by slow diffusion of *n*-hexane into a saturated acetone solution, the electronic requirements of the acidic $Ag^{I}$ ion are fulfilled without picking any acetone molecule. Nevertheless, the silver centre displays Ag-F interactions with the non-coordinating $BF_4^-$ counterion, showing Ag-F distances [d Ag(1)-F(3) = 2.696 Å (**4A**), d Ag(2)-F(6) = 2.684 Å (**4B**)] significantly larger than the sum of the covalent radii (2.08 Å)[88] and comparable to related compounds.[89-92] The coordination environment at the Ag(I) ion is illustrated in Figure 5. This scheme just takes into consideration Ag-Pt bonds and Ag-F interaction. As can be observed, the silver centre displays a distorted trigonal planar geometry with angles close to 120°. The silver atom deviates from the best plane formed by the atoms [Pt, F, Pt] by a distance of 0.090 Å in **4A** and 0.117 Å in **4B**.

Figure 5

Importantly, intramolecular π-π contacts are found between the pyridine rings of the CNC ligands within the same $Pt_2Ag$ cationic complex [d($Cg_1$–$Cg_2$) = 3.667 Å in **4A** and d($Cg_3$–$Cg_4$) = 3.579 Å in **4B**; *Cg* is the centroid of the pyridine ring in CNC ligand]).[59,60,73,77,82,83]
Unlike $[\{(tmeda)Pt(pz)_2\}_2Ag](ClO_4)_5$,[75] in which the silver ion is linearly joined to the N atoms of the pyrazine ligand, in compound **4** the Ag centre displays different electronic preferences, interacting with the platinum and aromatic electron densities.
The more shielded signals observed for $H^d$ (dmpyz) protons in **3** and **4** compared to **1** are in agreement with this structure, in which the *ortho*-hydrogens ($H^d$) are fairly close (< 3 Å) to the electron density of the M(I) ion. Unluckily, solutions of **3** either in acetone or $CH_2Cl_2$ are not stable enough to grow suitable crystals for X-ray diffraction. Based on the NMR and mass spectral data reported above and that for some related compounds with Pt(II)-Cu(I) dative bonds found in literature[14,93,94] we proposed a similar sandwich $Pt_2Cu$ structure for compound **3**.

**Photophysical properties of compounds 1-4**

***Absorption spectra and DFT calculations***

UV-Vis spectra data of compounds **1-4** are listed in Table 4. They all display structured bands at 350-375 nm ($\varepsilon > 10^4$ $M^{-1}cm^{-1}$) with vibronic differences (*ca*. 1300 $cm^{-1}$) in agreement with the skeletal frequency of the ligand C^N^C (see Figure 6). Compounds **1**, **3** and **4** show a

modest shoulder at around 400 nm ($\varepsilon \approx 3 \cdot 10^3$ $M^{-1}$ $cm^{-1}$) whereas the dinuclear complex **2** displays additional absorptions bands at lower energies 418 and 457 nm ($\varepsilon \approx 15 \cdot 10^3$ $M^{-1}cm^{-1}$). To determine if these bands were associated with intermolecular transitions, we acquired absorption spectra of **2** at concentrations ranging from $10^{-5}$ to $10^{-6}$ M. As shown in Figure S3, the absorptions at 418 and 452 nm obey Beer's Law, suggesting that they are due to transitions in the molecular species and no significant aggregation occurs within this concentration range.

Figure 6

UV-Vis spectra of **1**, **3** and **4** were recorded in different solvents showing a moderate solvatochromism, particularly more intense in the lower energy spectral region ($\lambda$ > 400 nm). For **1** the absorption maxima suffer a blue shift of *ca* 7 nm when increasing the polarity of solvents (Figure 7), which is characteristic of charge transfer (CT) transitions.[54] The same behavior was observed for compounds **3** and **4** (see Figure S4). Unlike other reported Pt-M compounds with Pt-M dative bonds,[14,17] **3** and **4** do not show any significant blue shift in $CH_2Cl_2$ solutions. The blue shift of the $^1$MLCT bands in compounds with Pt-M dative bonds is explained by an increase of electrophilicity of the Pt center, lowering the energy in the HOMO.

Figure 7

To better explain these assignments, time-dependent density functional theory (TD-DFT) calculations were carried out for **1** and **2** using the B3LYP hybrid density functional. The geometric parameters of the optimized structures (Tables S2 and S3) agree well with the experimental values. The molecular orbitals involved in the main excited states are depicted in Figures S6 and S7 and the relative compositions of the different energy levels are reported in Table 5. Calculated excited states for **1** and **2** are listed in Table 6. The selected allowed transitions are in agreement with the experimentally observed absorption maxima (Figure 8 and 9). TD-DFT calculations on **1** indicate that there is a considerable orbital mixing for the transitions. The two lowest energy calculated absorptions are 363 and 400 nm and they are involving the following transitions [HO-3 $\rightarrow$ LUMO (95%) for 363 nm] and [HO-1 $\rightarrow$ LU+1 (93%) for 400 nm]. As shown in Figure 8 and Table 5, the frontier orbitals implicated in these transitions are rather different, in particular the unoccupied orbitals: LU+1 is mostly constructed from orbitals located on the ancillary ligand (dmpyz, 87%) whereas the LUMO is

based on the tridentate CNC ligand (88%). The occupied orbitals, HO-1 (400 nm) and HO-3 (363 nm) are both mainly Pt and CNC based, they show different contributions of each other [HO-1: Pt (25 %), CNC (68 %) / HO-3: Pt (9 %), CNC (87 %)]. Therefore, the lower energy calculated absorption [HO-1 → LU+1 (93%) for 400 nm] may correspond to a mixed L'LCT [π(CNC) → π*(dmpyz)] / MLCT [5d(Pt) → π*(dmpyz)] transition while the 363 nm [HO-3 → LUMO] mainly correspond to a CNC ligand centered transition ($^1$LC R-C^N^C) mixed with a small MLCT character.

Figure 8, Figure 9

The calculated absorptions for complex **2** include the transitions [HO-2 → LUMO (98%) for 480 nm] and [HO-6 → LU+2 (46%) and HO-5 → LU+1 (49%) for 361 nm]. As is shown in Figure S7 and Table 5, HO-6 and HO-5 are both degenerated orbitals with almost identical contributions (CNC ligand, 91%), the same as LU+2 and LU+1, therefore in Figure 9, only a set of them are being depicted. All of the frontier orbitals involved in these two low energy transitions are basically the same to those observed in **1**. Therefore, the lower energy calculated absorption (480 nm) is assigned to a mixed L'LCT [π(CNC) → π*(dmpyz)] / MLCT [5d(Pt) → π*(dmpyz)] transition and the other one (361 nm) mainly correspond to a CNC ligand centered transition ($^1$LC R-C^N^C). It seems that the lowest energy absorptions in both complexes are exactly the same in nature although they differ in energy. These assignments are in concordance with other previously reported results.[59,60,73,77,81] The small contribution of the platinum center to all these transitions would explain why the UV-Vis spectra of the trinuclear compounds **3** and **4** do not suffer a significant blue shift compared to the starting material **1**.

Diffuse reflectance spectra of the solids **1**-**3** are depicted in Figure S5. Compounds **1** and **3** show additional absorptions (450-600 nm) when compared to their corresponding solution UV-Vis spectra. These low energy bands can be assigned to π···π interactions between the CNC fragments, as shown in the X-ray structures. Therefore, either in solid state or solution the Pt-M donor-acceptor bonds[71] do not seem to be involved in the molecular transitions.

***Emission Spectroscopy.***

Emission data for **1-4** are summarized in Table 7. All compounds are photoluminescent in the solid state and in 2-Methyltetrahydrofuran (2-MeTHF) glassy solutions (77 K) but none of them are emissive in either solid state or fluid solutions at room temperature. This is due to nonradiative processes concerning low lying *d-d* excited states and fast nonradiative decay rates, as a result of a large excited-state structural distortion.[72]

*Solid State*

In the solid state at 77 K, compounds **1-4** display broad and unstructured emissions at very low energies with rather short lifetimes (< 2 μs). As shown in Figure 10, emission bands in **3** ($\lambda_{max}$= 688 nm) and **4** ($\lambda_{max}$= 695 nm) are significantly enhanced (Inset Fig. 10) and blue shifted when comparing to the starting complex, **1** ($\lambda_{max}$= 720 nm). Upon M(I) coordination to the monomer, the non radiative processes seems to be reduced, giving more intense emissions in **3** and **4**. Complex **1** displays such a weak emission that the lifetime could not be measured properly. Excitation spectra of **1-4** are very similar, all of them show very low energy excitations with maxima at *ca.* 580 nm.

Figure 10

In accordance with the crystal structures of **1** and **2**, which show no Pt-Pt interactions but close π-π intermolecular contacts (see Figures 1b and 2b), the solid state emissive behavior (low energy broad bands, with no structure and short lifetimes) and the low energy excitations, emissions of **1** and **2** are assigned to $^3\pi\pi$ (R-CNC) excited states due to the ground-state aggregation of monomers.[56,59-62,73] Compounds **3** and **4** exhibit almost identical emission and excitation profiles. Therefore, on the basis of the crystal structure of **4**, which contains a trinuclear complex with Pt-Ag dative bonds and intramolecular π-π interactions only between the CNC rings within the cluster, both emissions are assigned to $^3\pi\pi$ (R-CNC) transitions perturbed by the M(I) ion. The intramolecular π-π contacts found in **4** (~ 3.6 Å) are slightly longer compared to those observed in **1** and **2** (< 3.4 Å), also **1** and **2** showed a supramolecular structure defined by these π-π interactions (Figures 1b and 2b). So, a less effective overlap of the CNC ligands in **4**, due to the inclusion of the $Ag^+$ ion, would produce a higher energy gap [π(CNC) → π*(CNC)], which is consistent with the blue shifted emission observed.

*Glassy Solution State*

Emissive behavior of **1-4** in 2-MeTHF solutions at 77 K is completely different from the solid state data. Also, compound **3** exhibits very similar emissions to those observed for the monomer, **1** (see Figure S8), which is in agreement with the results obtained from the Pt NMR experiments at 193 K. Therefore, as both techniques, NMR and photoluminescence, confirm the Pt-Cu core falls apart in solutions at low temperatures (T < 193 K), the photophysical study of **3** in glassy solution (77 K) was not undertaken.

Diluted solutions ($5 \cdot 10^{-5}$ M) of **1** and **2** in 2-MeTHF at 77 K show analogous emission bands which are particularly sensitive to the excitation wavelengths. They both exhibit a highly structured band with maxima at 490 nm upon exciting with $\lambda_{ex}$ < 400 nm (Figure 11, top). The vibrational spacings are ca. 1350-1500 $cm^{-1}$ corresponding to C=C / C=N stretches of the R-C^N^C or dmpyz, suggesting the involvement of these in the emissive state. Complex **1** revealed an odd increase of the intensity in the ~ 560 nm peak compared to that in **2**. Excitation spectra of **1** and **2** monitored at $\lambda_{em}$ = 490 nm are essentially the same and fit reasonably well with the UV-Vis spectrum of **1**. Upon excitation with $\lambda_{ex}$ > 400 nm there is a dramatic change in the emission profiles of **1** and **2**, whereby a different but also structured band becomes predominant (Figure 11, bottom).

Figure 11

This new emission band appears at lower energies with maxima at 556 nm (LE, 556 and 600 nm) showing vibrational spacings of *ca*. 1300 $cm^{-1}$ characteristic of the R-C^N^C or dmpyz ligands. Emission spectra in **1** and **2** barely show the high energy HE band (490 nm, 525 nm). Excitation spectra of **1** and **2** recorded at $\lambda_{em}$ = 556 nm are identical and they also undergo a shift to lower energies.

This wavelength-dependent behavior has been previously observed in related neutral complexes with the same R-C^N^C tridentate ligand [(R-C^N^C)Pt(L)].[73] Lifetimes measurements registered on **1** at the HE band fit to only one component ($\tau$ ~ 27 $\mu$s). However, the measurements corresponding to the LE band lead to two different components ($\tau$ ~ 17.7 and 4.5 $\mu$s). Therefore, from all these data, and considering the TD-DFT calculations, the HE (490, 525 nm) band is assigned to metal perturbed $^3$ILCT excited states involving the R-CNC ligand, since its long lifetimes and highly structured profiles are typical of "Pt(CNC)" monomers.[59,60,73,77,80] The LE (~ 556, 600 nm) band displays two different lifetimes, which

suggests the presence of two close emissive states. According to the excitation spectra, vibronic profiles, TD-DFT calculations and the lifetimes values, the longer one (~ 18 μs) is attributed to $^3$L'LCT / $^3$MLCT transitions and the shorter one (~ 4 μs) is tentatively associated to the formation of aggregates in the ground state. Both emissive states are related to the R-CNC ligand.[59,60,73,77,80]

The Pt-Ag derivative (**4**) exhibits a completely different emission profile in diluted glassy solutions ($5 \cdot 10^{-5}$ M). As shown in Figure 11, a broad unstructured band appears at very low energy (680 nm) along with a shoulder at 556 nm. The emission profile is not dependent on the $\lambda_{ex}$. The lifetime of the 680 nm band fits to a monoexponential decay ($\tau$ ~ 0.6 μs); this band only observed in the Pt-Ag derivative (**4**) is very similar to the solid state emissions of **1-4**, and is attributed to $^3\pi\pi$ (R-CNC) excimeric transitions as a result of intramolecular π-π contacts between the CNC ligands within the cluster structure. The shoulder at 556 nm fits two components ($\tau$ ~ 16.7 and 6.6 μs); these values along with the emission energy are very similar to those obtained for **1**, and the same assignment seems plausible.

Due to solubility issues found in **1** and especially in **2,** experiments in concentrated ($10^{-3}$ M) solutions could not be performed. Compound **4** (Table 7) behaves in the same manner as in diluted solutions, it **4** shows exactly the same emissions (559 and 680 nm) observed in diluted solutions or in solid state. Therefore, the assignments of these are the same as those discussed above.

## Concluding Remarks

The mononuclear complex [($EtO_2$C-C^N^C)Pt(dmpyz)] (**1**) has been synthesised and used as a building block to prepare the homodinuclear complex [{($EtO_2$C-C^N^C)Pt}$_2$($\mu$-dmpyz)] (**2**) and the heterotrinuclear clusters [{($EtO_2$C-C^N^C)Pt(dmpyz)}$_2$M]$^+$ (M= Cu (**3**) and Ag(**4**)). Upon coordination to the Pt center, the free N of the monotopic dmpyz in **1** exhibited reduced basicity. This is supported by the increasing inertia noticed in formation of **2** and by the preference of the acidic metal center Ag(I) towards the Pt electron density rather than the lone pair of electrons on the non-coordinated nitrogen atom in the dmpyz ligand. Therefore, to our knowledge, compounds **3** and **4** are the first examples of $Pt_2M$ clusters displaying Pt-M dative bonds with a tridentate biscyclometalated ligand. Crystal structure of **4** shows two [$Pt_2$Ag] sandwich-type clusters in the asymmetric unit, both with the two square–planar "(R-CNC)Pt(dmpyz)" moieties stabilized by two Pt→Ag donor-acceptor bonds as well as by $\eta^1$- and $\eta^2$-Ag-C interactions. Intra (**4**) and intermolecular (**1** and **2**) π-π contacts between the aromatic rings of the CNC ligands were found in their crystal structures. The $Pt_2M$ core structure is also retained in solution at room temperature since it has been confirmed by $^1$H and $^{195}$Pt NMR spectroscopy and mass spectrometry. Their $^{195}$Pt NMR spectra at room temperature show broad singlets significantly downfield shifted (160 (**3**) and 250 ppm (**4**)) when comparing to monomer (**1**), which is due to presence of Pt-M dative bonds. Even at temperatures of 223 K, the $^{195}$Pt NMR spectrum of **3** still exhibits the signal due to the trinuclear $Pt_2Cu$ species. At lower temperatures (T = 193 K), the copper derivative definitely falls apart, whereas the silver one still holds up unbroken. $^{195}$Pt NMR spectrum of **4** at 193 K exhibits the expected doublet because of the coupling to the spin active $^{107,109}$Ag nuclei. Photophysical experiments on **1**-**4** support the conclusions drawn from the X-ray and NMR studies. In solid state compounds **1**-**4** give red emissions arising from $^3$ππ excited states due to the intra- or intermolecular π-π contacts (CNC). Diluted 2-MeTHF glassy solutions (77 K) of complexes **1** and **2** show structured emission bands which are particularly sensitive to the λex, the HE (490, 525 nm) band due to metal perturbed $^3$ILCT (CNC) excited states and LE one (556, 600 nm), which fits two different lifetimes, is associated to the formation of aggregates in the ground state and to $^3$L'LCT/$^3$MLCT transitions. In contrast, **4** displays mainly an unstructured emission at 680 nm independent on the $\lambda_{ex}$, which is related to the solid state emission. As expected, compound **3** displays analogous emissions to those from the monomer **1**, proving the $Pt_2Cu$ core to be broken at this temperature (77 K).

## Experimental Section

**General Comments.** Information describing materials, instrumental methods used for characterization, photophysical and spectroscopic studies, computational details concerning TD-DFT calculations and X-ray structures are contained in the Supporting Information. All chemicals were used as supplied unless stated otherwise. $[Cu(MeCN)_4]PF_6$[95] and [($EtO_2C$-C^N^C)Pt(DMSO)] (A)[73] were prepared by literature methods.

**Preparation of [(EtOOC-C^N^C)Pt(dmpyz)] (1).** 2,5-dimethylpyrazine (150 $\mu$L, 0.92 mmol) was added to a solution of [(EtOOC-C^N^C)Pt(DMSO)] (**A**) (200 mg, 0.35 mmol) in dichloromethane (15 mL). After stirring for 16 h at room temperature, the solvent was evaporated to 2 mL and methanol (15 mL) was added to render an orange solid. The mixture was stirred for 1 h and air filtered. Yield: 176 mg, 84%. Anal. Calcd for $C_{26}H_{23}N_3O_2Pt$: C, 51.64; H, 3.83; N, 6.95. Found: C, 51.29; H, 3.75; N, 6.70. IR (ATR, $cm^{-1}$) $\nu$(COOEt): 1718 (s). MS-ESI (+): m/z: 605 $[M]^+$. $^1$H NMR plus HMBC and HSQC (500 MHz, $CD_2Cl_2$, 293 K): $\delta$ 8.87 (s, $^3J_{H\text{-}Pt}$ = 49.0, $H^d$, dmpyz), 8.58 (s, $^4J_{H\text{-}Pt}$ = 15.5, $H^b$, dmpyz), 7.80 (s, $^4J_{H\text{-}Pt}$ = 8.0, 2H, $H^8$), 7.56 (d, $^3J_{H\text{-}H}$ = 7.5, 2H, $H^5$), 7.15 (td, $^3J_{H\text{-}H}$ = 7.5; $^4J_{H\text{-}H}$ = 1.5, 2H, $H^3$), 7.08 (td, $^3J_{H\text{-}H}$ = 7.5; $^4J_{H\text{-}H}$ = 1.5, 2H, $H^4$), 6.73 (dd, $^3J_{H\text{-}H}$ = 7.5; $^4J_{H\text{-}H}$ = 1.5; $^3J_{H\text{-}Pt}$ = 32.0, 2H, $H^2$), 4.45 (q, $^3J_{H\text{-}H}$ = 7.0, 2H, $OCH_2$), 2.67 (s, $^4J_{H\text{-}Pt}$ = 9.0, 3H, $Me^a$, dmpyz), 2.58 (s, 3H, $Me^c$, dmpyz), 1.45 (t, $^3J_{H\text{-}H}$ = 7.0, 3H, $OCH_2\mathit{CH}_3$). $^{13}C\{^1H\}$ NMR plus HMBC and HSQC (125.7 MHz, $CD_2Cl_2$, 293 K): $\delta$ 170.5 (s, $^1J_{C\text{-}Pt}$ = 729.2, 2C, $C^1$), 168.5 (s, $^2J_{C\text{-}Pt}$ = 77.1, 2C, $C^7$), 164.6 (s, *C*OOEt), 153.4 (s, $^3J_{C\text{-}Pt}$ = 48.9, $C^c$, dmpyz), 151.2 (s, $C^a$, dmpyz), 148.3 (s, $^2J_{C\text{-}Pt}$ = 55.9, 2C, $C^6$), 146.9 (s, $^3J_{C\text{-}Pt}$ = 28.6, $C^b$, dmpyz), 145.1 (s, $C^d$, dmpyz), 141.2 (s, $C^9$), 133.8 (s, $^2J_{C\text{-}Pt}$ = 46.7, 2C, $C^2$), 130.9 (s, $^4J_{C\text{-}Pt}$ = 29.5, 2C, $C^3$), 124.4 (s, $^3J_{C\text{-}Pt}$ = 28.6, 2C, $C^5$), 123.8 (s, 2C, $C^4$), 114.1 (s, $^3J_{C\text{-}Pt}$ = 39.3, 2C, $C^8$), 62.1 (s, $OCH_2$), 23.9 (s, $^3J_{C\text{-}Pt}$ = 66.6, $Me^a$, dmpyz), 20.8 (s, $Me^c$, dmpyz), 14.0 (1C, s, $OCH_2\mathit{CH}_3$). $^{195}Pt\{^1H\}$ NMR (107.1 MHz, $CD_2Cl_2$, 293 K): $\delta$ - 3490

**Preparation of [{(EtOOC-C^N^C)Pt}$_2$($\mu$-dmpyz)] (2).** A mixture of **A** (300 mg, 0.52 mmol) and 2,5-dimethylpyrazine (28 $\mu$L, 0.26 mmol) in dichloromethane (10 mL) was stirred for 4 days at room temperature. The resultant suspension was filtered and the solid was washed with dichloromethane and diethyl ether. Yield: 171 mg, 60%. Anal. Calc. for $C_{46}H_{38}N_4O_4Pt_2$: C, 50.18; H, 3.48; N, 5.08. Found: C, 49.7; H, 3.40; N, 4.97. IR (ATR, $cm^{-1}$) $\nu$(COOEt): 1719 (s). MS-ESI (+): m/z: 1100 $[M]^+$. $^1$H NMR (500 MHz, $CD_2Cl_2$, 293 K): $\delta$ 9.14 (s, $^3J_{H\text{-}Pt}$ = 49.0, 2H, $H^d$ = $H^b$, dmpyz), 7.84 (s, 4H, $H^8$), 7.61 (d, $^3J_{H\text{-}H}$ = 7.5, 4H, $H^5$), 7.28 (t, $^3J_{H\text{-}H}$ = 7.5, 4H, $H^3$), 7.15 (t, $^3J_{H\text{-}H}$ = 7.5, 4H, $H^4$), 6.91 (d, $^3J_{H\text{-}H}$ = 7.5, $^3J_{H\text{-}Pt}$ = 25.0, 4H, $H^2$), 4.46 (q, $^3J_{H\text{-}H}$ = 7.0, 4H, $OCH_2$), 2.72 (s, 6H, Me, dmpyz), 1.47 (t, $^3J_{H\text{-}H}$ = 7.0, 6H,

$OCH_2CH_3$). $^{13}C\{^1H\}$ NMR spectrum not able to record due to its low solubility. $^{195}Pt\{^1H\}$ NMR (107.1 MHz, $CD_2Cl_2$, 293 K): δ - 3461

**Preparation of [{(EtOOC-C^N^C)Pt(dmpyz)}$_2$Cu]PF$_6$ (3).** $[Cu(MeCN)_4]PF_6$ (50 mg, 0.135 mmol) was added to an orange solution of **1** (164 mg, 0.27 mmol) in dichloromethane (20 mL) at r.t. After 1 h stirring, the resulting mixture was evaporated to dryness. Addition of diethyl ether (3 x 5 mL) to the residue rendered a deep orange solid which was filtered and vacuum dried. Yield: 159 mg, 83%. Anal. Calc. for $C_{52}H_{46}CuPF_6N_6O_4Pt_2$: C, 44.05; H, 3.27; N, 5.92. Found: C, 44.38; H, 3.21; N, 5.52. IR (ATR, $cm^{-1}$) $\nu$(COOEt): 1719 (s); $\nu$($PF_6$): 832 (vs). MS-ESI (+): m/z: 1272.2 $[M]^+$. $^1H$ NMR (500 MHz, Acetone-$d^6$, 293 K): δ 8.79 (s, $^4J_{H\text{-}Pt}$ = 12.0, 2H, $H^b$, dmpyz), 8.57 (s, br, 2H, $H^d$, dmpyz), 7.79 (s, 4H, $H^8$), 7.71 (d, $^3J_{H\text{-}H}$ = 7.5, 4H, $H^5$), 7.26 (td, $^3J_{H\text{-}H}$ = 7.5; $^4J_{H\text{-}H}$ = 1.0, 4H, $H^4$), 7.21 (td, $^3J_{H\text{-}H}$ = 7.5; $^4J_{H\text{-}H}$ = 1.0, 4H, $H^3$), 6.75 (d, $^3J_{H\text{-}H}$ = 7.5; $^3J_{H\text{-}Pt}$ = 27.5, 4H, $H^2$), 4.53 (q, $^3J_{H\text{-}H}$ = 7.0, 4H, $OCH_2$), 2.62 (s, 6H, Me, dmpyz), 2.61 (s, 6H, Me, dmpyz), 1.53 (t, $^3J_{H\text{-}H}$ = 7.0, 6H, $OCH_2CH_3$). Compound **3** is not stable enough to record the $^{13}C\{^1H\}$ NMR spectrum. $^{19}F$ NMR (470.5 MHz, Acetone-$d^6$, 293 K): δ -72.0 (d, $^1J_{F\text{-}P}$ = 708.2, $PF_6$). $^{195}Pt\{^1H\}$ NMR (107.1 MHz, $CD_2Cl_2$, 293 K): δ - 3330

**Preparation of [{(EtOOC-C^N^C)Pt(dmpyz)}$_2$Ag]BF$_4$ (4).** $AgBF_4$ (19 mg, 0.097 mmol) was added to an orange suspension of **1** (120 mg, 0.19 mmol) in acetone (20 mL) at r.t. After 1 h stirring, the resulting red solution was filtered through celite and evaporated to dryness. Addition of diethyl ether (15 mL) to the residue rendered a red crystalline solid which was filtered. Yield: 115 mg, 82%. Anal. Calcd. for $C_{52}H_{46}AgBF_4N_6O_4Pt_2$: C, 44.49; H, 3.30; N, 5.98. Found: C, 44.70; H, 3.26; N, 5.45. IR (ATR, $cm^{-1}$) $\nu$(COOEt): 1720 (s); $\nu$($BF_4$): 1030 (vs, br). MS-ESI (+): m/z: 1317.2 $[M]^+$. $^1H$ NMR plus HMBC and HSQC (500 MHz, Acetone-$d^6$, 293 K): δ 8.70 (s, $^4J_{H\text{-}Pt}$ = 11.0, 2H, $H^b$, dmpyz), 8.20 (s, $^3J_{H\text{-}Pt}$ = 50.5, 2H, $H^d$, dmpyz), 7.64 (d, $^3J_{H\text{-}H}$ = 7.5, 4H, $H^5$), 7.60 (s, 4H, $H^8$), 7.29 (td, $^3J_{H\text{-}H}$ = 7.5; $^4J_{H\text{-}H}$ = 1.0, 4H, $H^4$), 7.22 (td, $^3J_{H\text{-}H}$ = 7.5; $^4J_{H\text{-}H}$ = 1.0, 4H, $H^3$), 6.69 (d, $^3J_{H\text{-}H}$ = 7.5; $^3J_{H\text{-}Pt}$ = 20.0, 4H, $H^2$), 4.53 (q, $^3J_{H\text{-}H}$ = 7.0, 4H, $OCH_2$), 2.56 (s, 6H, $Me^c$, dmpyz), 2.48 (s, $^4J_{H\text{-}Pt}$ = 9.6, 6H, $Me^a$, dmpyz), 1.53 (t, $^3J_{H\text{-}H}$ = 7.0, 6H, $OCH_2CH_3$). $^{13}C\{^1H\}$ NMR plus HMBC and HSQC (125.7 MHz, Acetone-$d^6$, 293 K): δ 168.4 (s, $^2J_{C\text{-}Pt}$ = 72.3, 4C, $C^7$), 164.4 (s, 2C, *C*OOEt), 156.1 (s, 4C, $C^1$), 155.1 (s, $^3J_{C\text{-}Pt}$ = 50.5, 2C, $C^c$, dmpyz), 152.4 (s, 2C, $C^a$, dmpyz), 151.4(s, $^2J_{C\text{-}Pt}$ = 57.9, 4C, $C^6$), 149.0 (s, $^3J_{C\text{-}Pt}$ = 26.3, 2C, $C^b$, dmpyz), 146.4 (s, 2C, $C^d$, dmpyz), 143.3 (s, 2C, $C^9$), 136.4 (s, $^2J_{C\text{-}Pt}$ = 53.5, 4C, $C^2$), 132.4 (s, $^4J_{C\text{-}Pt}$ = 25.9, 4C, $C^3$), 128.3 (s, 4C, $C^4$), 126.4 (s, $^3J_{C\text{-}Pt}$ = 25.9, 4C, $C^5$), 116.1 (s, $^3J_{C\text{-}Pt}$ = 35.9, 4C, $C^8$), 63.2 (s, 2C, $OCH_2$), 24.8 (s, $^3J_{C\text{-}Pt}$ = 55.3,

2C, $Me^a$, dmpyz), 21.7 (s, 2C, $Me^c$, dmpyz), 14.6 (s, 2C, $OCH_2\mathit{CH_3}$). $^{19}F$ NMR (470.5 MHz, Acetone-$d^6$, 293 K): δ -151.9 (s, $BF_4$). $^{195}Pt\{^1H\}$ NMR (107.1 MHz, $CD_2Cl_2$, 293 K): δ -3240

**Acknowledgments:** The authors gratefully acknowledge the European Commission for financial support under the Marie Curie Intra-European Fellowship (PIEF-GA-2009-252883; SFL-PRR) and Prof. Juan Fornies (University of Zaragoza, Spain) for the use of facilities to do the photophysical studies. The support of the Engineering and Physical Sciences Research Council (UK) is also acknowledged and particularly for their award of a Senior Fellowship to PRR and studentships to CHW.

**Supporting information available:** General procedures, computational and crystallographic details. Xray structure analysis of **1**, **2·$CH_2Cl_2$** and **4** (Table S1). Experimental and calculated ESI-MS spectrum of **3** and **4** in MeCN solution (Fig. S1 and S2). UV-Vis spectra of complex **2** at different concentrations; Linear fit (Fig. S3). Normalized UV-Vis spectra of compound **3** (Fig. S4). Normalized Diffuse Reflectance spectra of **1**-**3** in solid state (Fig. S5). Tables of atomic coordinates of compounds **1** and **2** (S2, S3) and pictures of the representative frontier orbitals for them (Fig. S6 and S7). Emission spectra of diluted glassy solutions of **1** and **3** (Fig. S8). Crystallographic data in CIF format.

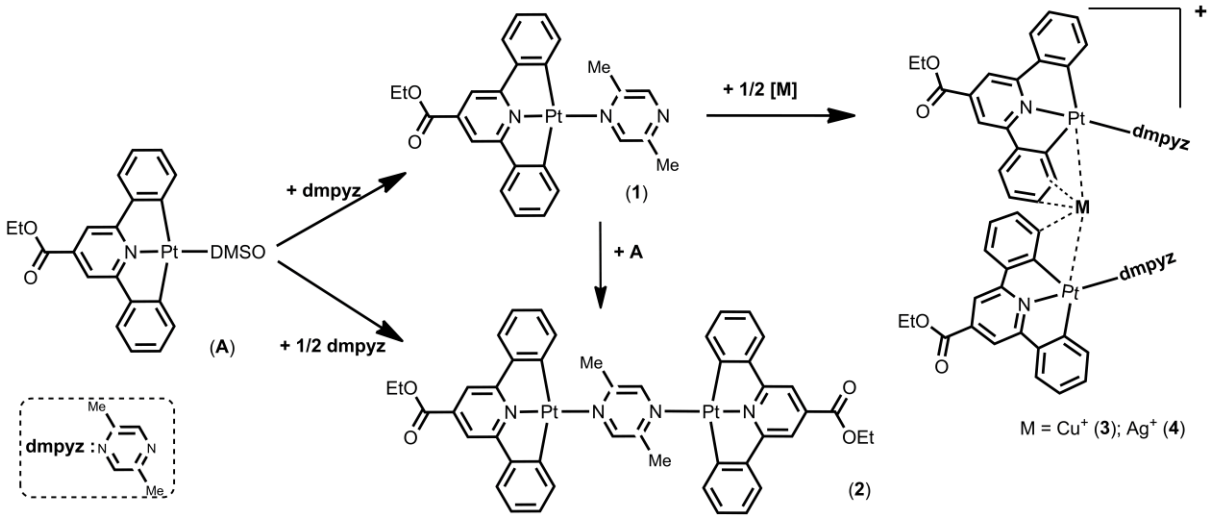


Scheme 1

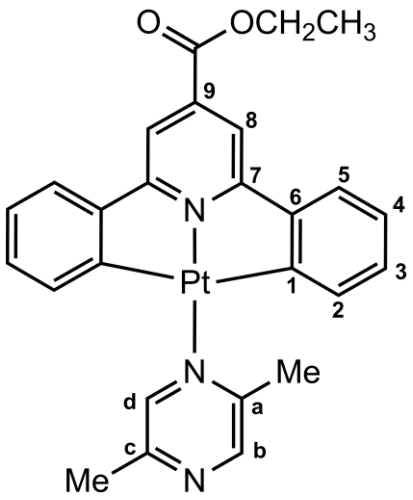


Scheme 2

**Table 1**. Selected bond lengths (Å) and angles (º) for complexes **1** and **2·$CH_2Cl_2$**

| **1** | | **2·$CH_2Cl_2$** | |
|---|---|---|---|
| Distances (Å) | | | |
| Pt(01)-C(11) | 2.048(6) | Pt(1)-C(11) | 2.042(8) |
| Pt(01)-C(21) | 2.068(7) | Pt(1)-C(21) | 2.046(8) |
| Pt(1)-N(1) | 1.962(5) | Pt(1)-N(1) | 1.963(5) |
| Pt(1)-N(2) | 2.018(6) | Pt(1)-N(2) | 2.016(5) |
| C(4)-C(7) | 1.485(11) | C(4)-C(7) | 1.481(9) |
| C(7)-O(1) | 1.217(8) | C(7)-O(1) | 1.215(9) |
| C(8)-C(9) | 1.483(11) | C(8)-C(9) | 1.491(14) |
| C(7)-O(2) | 1.329(8) | C(7)-O(2) | 1.329(10) |
| | | Pt(2)-C(51) | 2.035(8) |
| | | Pt(2)-C(61) | 2.045(8) |
| | | Pt(2)-N(4) | 1.972(5) |
| | | Pt(2)-N(3) | 2.004(5) |
| Angles (º) | | | |
| C(11)-Pt(01)-C(21) | 162.9(3) | C(11)-Pt(1)-C(21) | 162.4(3) |
| N(1)-Pt(01)-C(21) | 81.5(2) | N(1)-Pt(1)-C(21) | 81.3(3) |
| N(1)-Pt(01)-C(11) | 81.4(2) | N(1)-Pt(1)-C(11) | 81.2(2) |
| C(11)-Pt(01)-N(2) | 98.6(2) | C(11)-Pt(1)-N(2) | 98.9(2) |
| C(21)-Pt(01)-N(2) | 98.5(2) | C(21)-Pt(1)-N(2) | 98.6(3) |
| | | C(51)-Pt(2)-C(61) | 162.7(3) |
| | | N(4)-Pt(2)-C(61) | 81.3(3) |
| | | N(4)-Pt(2)-C(51) | 81.4(3) |
| | | C(51)-Pt(2)-N(3) | 98.6(2) |
| | | C(61)-Pt(1)-N(3) | 98.6(3) |

**Table 2.** $^{195}Pt\{^{1}H\}$ NMR data for complexes **1**-**4** in dichloromethane-$d^2$

| Compd | 293 K | 193 K |
|---|---|---|
| **1** | -3490 / -3522[a] | -3523 |
| **2** | -3461 | [b] |
| **3** | -3330 | -3500, -3525 / -3544[a] |
| **4** | -3240 | -3272, -3525 / -3300[a] |

a) acetone-$d^6$; b) Not soluble enough

**Table 3**. Selected bond lengths (Å) and angles (º) for cation complexes **4A** and **4B**.

| **4A** | | **4B** | |
|---|---|---|---|
| Distances (Å) | | | |
| Pt(1)-Ag(1) | 2.7734(11) | Pt(3)-Ag(2) | 2.8072(12) |
| Pt(2)-Ag(1) | 2.9596(11) | Pt(4)-Ag(2) | 2.9098(12) |
| Pt(1)-C(11) | 2.047(10) | Pt(3)-C(91) | 2.011(14) |
| Pt(1)-N(1) | 1.979(8) | Pt(3)-N(7) | 1.884(12) |
| Pt(1)-N(2) | 2.035(8) | Pt(3)-N(8) | 2.043(11) |
| Pt(1)-C(21) | 2.094(11) | Pt(3)-C(101) | 2.115(10) |
| Pt(2)-C(51) | 2.053(10) | Pt(4)-C(131) | 2.069(10) |
| Pt(2)-N(4) | 1.971(9) | Pt(4)-N(10) | 1.953(8) |
| Pt(2)-N(5) | 2.031(8) | Pt(4)-N(11) | 2.034(9) |
| Pt(2)-C(61) | 2.058(11) | Pt(4)-C(141) | 2.034(11) |
| Ag(1)-C(21) | 2.317(11) | Ag(2)-C(101) | 2.315(12) |
| Ag(1)-C(51) | 2.283(10) | Ag(2)-C(131) | 2.299(13) |
| Ag(1)-C(56) | 2.591(11) | Ag(2)-C(136) | 2.655(12) |
| Angles (º) | | | |
| C(11)-Pt(1)-C(21) | 162.7(4) | C(91)-Pt(3)-C(101) | 162.5(6) |
| C(51)-Pt(2)-C(61) | 162.0(5) | C(131)-Pt(4)-C(141) | 161.7(4) |
| Pt(1)-Ag(1)-Pt(2) | 127.48(4) | Pt(3)-Ag(2)-Pt(4) | 130.49(4) |

**Table 4**. Absorption Data in $CH_2Cl_2$ solutions ($10^{-5}$ M) for compounds **1-4** at 298 K

| Compound | λ abs / nm ($10^3$ ε $M^{-1}cm^{-1}$) |
|---|---|
| **1** | 228 (24,7), 254 (21,4), 278 (29,9), 353 (11,7), 369 (13,4), 402 (3,7) tail to 550 |
| **2** | 229 (72,7), 253 (60,2), 277 (77,9), 308 (sh, 19,3), 355 (25,1), 369 (30,3), 418 (19,3), 457 (sh, 15,2) tail to 600 |
| **3** | 228 (54,6), 253 (50,1), 282 (45,0), 356 (17,6), 367 (18,6), 403 (4,8) tail to 550 |
| **4** | 228 (57,1), 253 (30,1), 277 (37,1), 357 (12,3), 367 (12,7), 401 (3,3) tail to 550 |

**Table 5**. Population Analysis (%) of Frontier MOs in the Ground State for **1** and **2**.

| MO | eV | | Pt | | R-C^N^C | | dmpyz | |
|---|---|---|---|---|---|---|---|---|
| | **1** | **2** | **1** | **2** | **1** | **2** | **1** | **2** |
| LU+5 | | -1.18 | | 2 | | 16 | | 82 |
| LU+4 | | -1.28 | | 1 | | 99 | | |
| LU+3 | | -1.29 | | 1 | | 80 | | 19 |
| LU+2 | -1.18 | -2.16 | 1 | 6 | 96 | 92 | 1 | 2 |
| LU+1 | -1.98 | -2.18 | 5 | 6 | 8 | 91 | 87 | 3 |
| LUMO | -2.07 | -2.51 | 6 | 10 | 88 | 10 | 6 | 80 |
| HOMO | -5.24 | -5.37 | 39 | 37 | 54 | 63 | | |
| HO-1 | -5.60 | -5.37 | 25 | 37 | 68 | 63 | 6 | |
| HO-2 | | -5.62 | | 29 | | 66 | | 5 |
| HO-3 | -6.03 | | 9 | | 87 | | | |
| HO-4 | -6.19 | | 26 | | 65 | | 1 | |
| HO-5 | | -6.14 | | 9 | | 91 | | |
| HO-6 | | -6.14 | | 9 | | 91 | | |
| HO-8 | | -6.31 | | 23 | | 76 | | 1 |
| HO-9 | | -6.31 | | 20 | | 79 | | 1 |

**Table 6**. Selected singlet excited states calculated by TD-DFT for complexes **1** and **2**.

| $\lambda_{exc}$ (calc.)/nm | o.s. | Transition (Percentage contribution) |
|---|---|---|
| **[(R-C^N^C)Pt(dmpyz)] (1)** | | |
| 400.14 | 0.1371 | HO-1 → LU+1 (93%) |
| 363.05 | 0.1004 | HO-3 → LUMO (95%) |
| 349.42 | 0.0393 | HO-4 → LUMO (44%); HOMO → LU+2 (38%) |
| **[{(R-C^N^C)Pt}$_2$($\mu$-dmpyz)] (2)** | | |
| 480.59 | 0.5177 | HO-2 → LUMO (98%) |
| 361.81 | 0.1869 | HO-6 → LU+2 (46%); HO-5 → LU+1 (49%) |
| 349.56 | 0.0749 | HOMO → LU+3 (36%); HO-8 → LU+1 (19%); HO-9 → LU+2 (18%); HOMO → LU+5 (11%) |

**Table 7.** Emission Data for complexes **1**-**4**

| Compound | Media/77 K | $\lambda_{em}$ (nm) | $\tau$ ($\mu$s) |
|---|---|---|---|
| **1** | Solid | 720 ($\lambda_{ex}$ 400-580) | a |
| | 2-MeTHF$_d$ | 490$_{max}$, 529, 560, 600 ($\lambda_{ex}$ <400) | 27.0 (490) |
| | | 491$_{sh}$, 556$_{max}$, 600, *t* to 750 ($\lambda_{ex}$ > 400) | 17.7 (16%), 4.5 (84%) (556) |
| **2** | Solid | 710 ($\lambda_{ex}$ 400-580) | 0.12 |
| | 2-MeTHF$_d$ | 490$_{max}$, 527, 560, 600 ($\lambda_{ex}$ <400) | |
| | | 491$_{sh}$, 556$_{max}$, 600, *t* to 750 ($\lambda_{ex}$ > 400) | |
| **3** | Solid | 688 ($\lambda_{ex}$ 400-590) | 1.8 |
| | 2-MeTHF$_d$ | 493$_{max}$, 525, 559 *t* to 700 ($\lambda_{ex}$ <400) | 25.5 (493) |
| **4** | Solid | 695 ($\lambda_{ex}$ 400-575) | 1.1 |
| | 2-MeTHF$_d$ | 556, 680 $_{max}$ ($\lambda_{ex}$ 360-500) | 0.6 (680) |
| | | | 16.7 (69%), 6.6 (31%) (556) |
| | 2-MeTHF$_c$ | 559, 682 $_{max}$ ($\lambda_{ex}$ 360-500) | |

a = too weak to be measured; *c* = $10^{-3}$M; *d* = 5 x $10^{-5}$M; *t* = tail

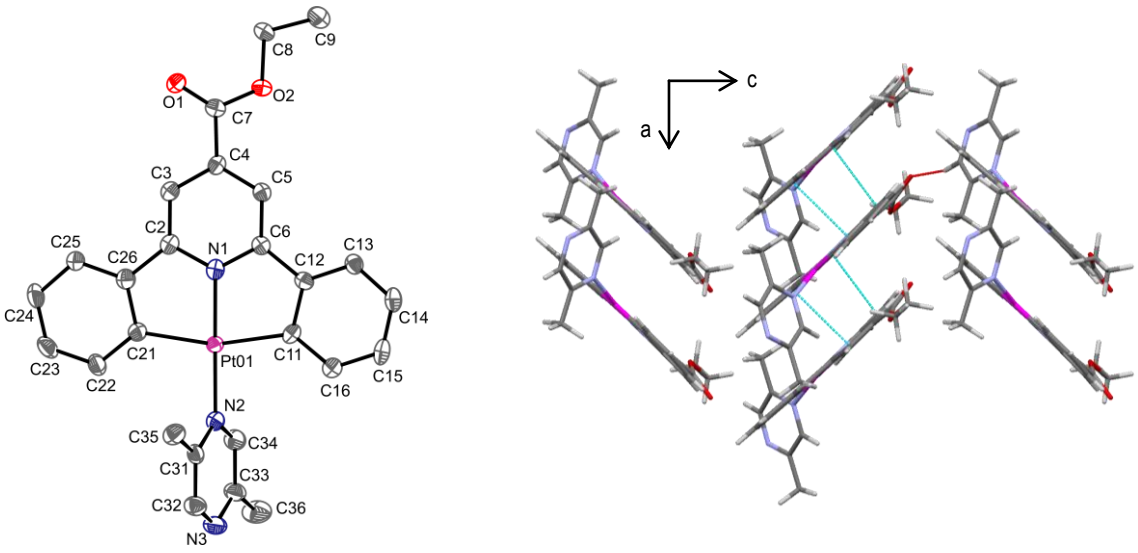


**Figure 1.** a) ORTEP view of **1**. Ellipsoids are drawn at the 50% probability level. Hydrogen atoms have been omitted for clarity. b) Crystal packing view of **1** along b axis.

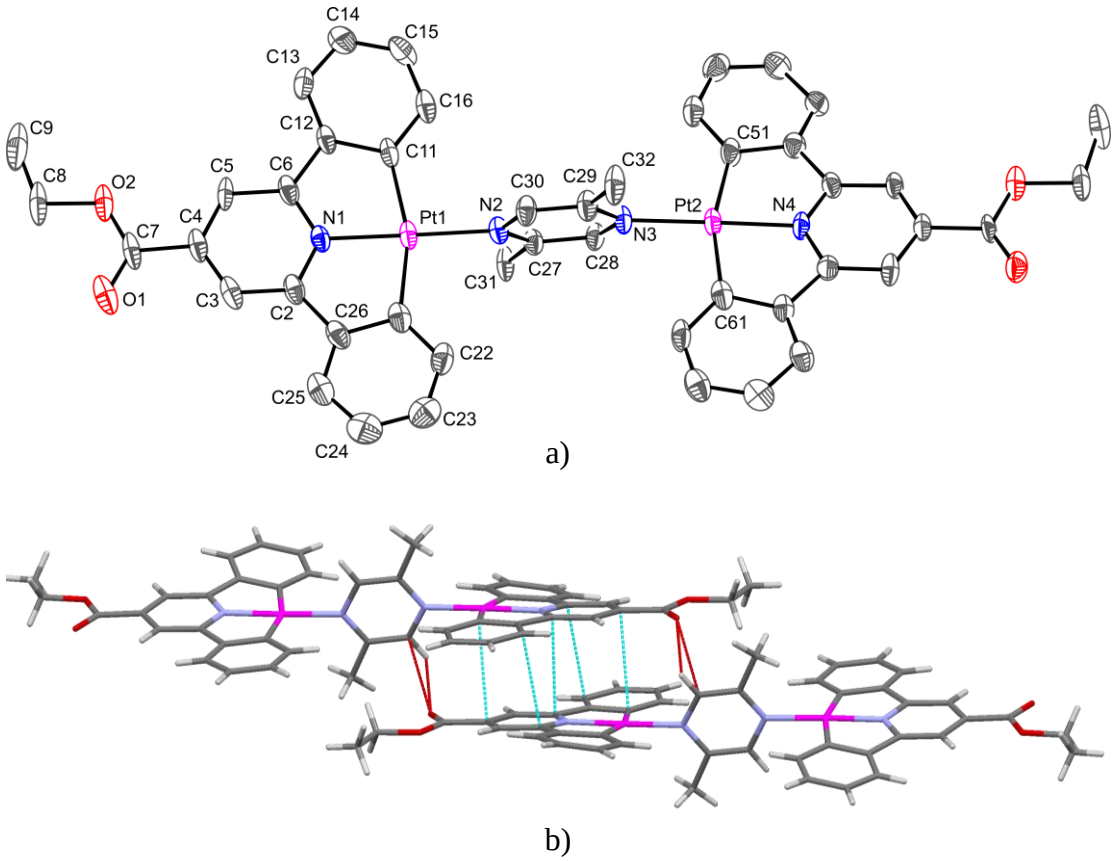


**Figure 2**. ORTEP view of **2**. Ellipsoids are drawn at the 50% probability level. Hydrogen atoms and solvent molecules have been omitted for clarity. b) Crystal packing diagram.

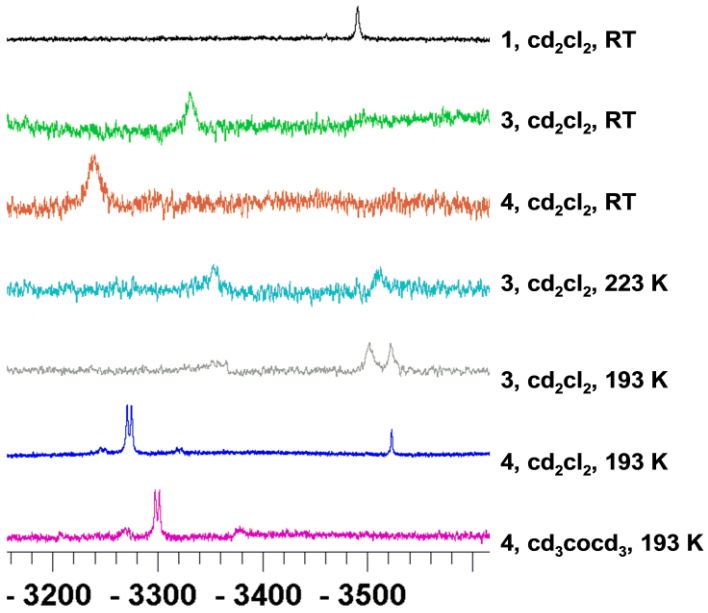


**Figure 3.** $^{195}Pt\{^{1}H\}$ NMR spectra of compounds **1**, **3** and **4**.

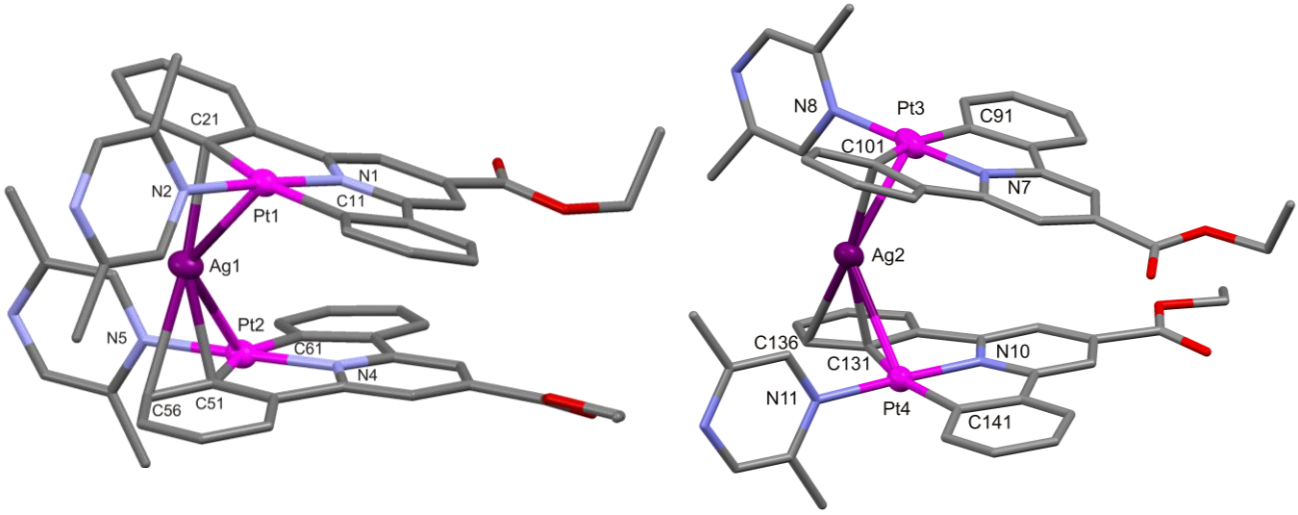


(a) (b)

**Figure 4.** Molecular structure views of the **4A** (a) and **4B** (b) cationic complexes. Hydrogen atoms and $BF_4$ anions have been omitted for clarity.

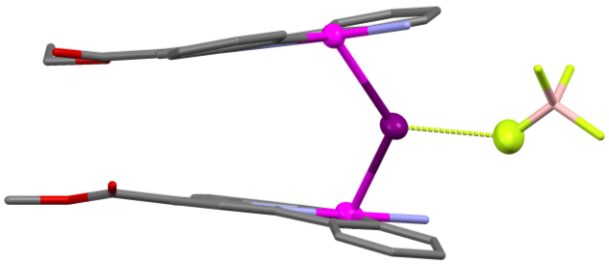

**Figure 5.** Representative coordination environment at the silver (I) ion in **4B**.

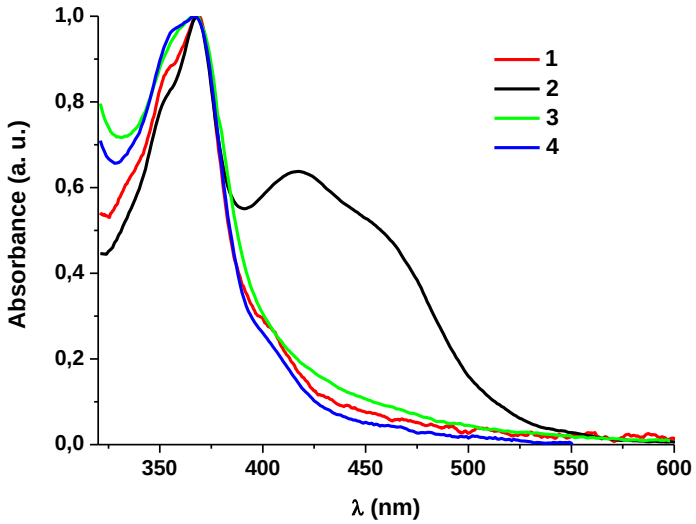


**Figure 6.** UV-Vis absorption spectra of complexes **1-4** in $CH_2Cl_2$ ($10^{-5}$ M) at 298 K

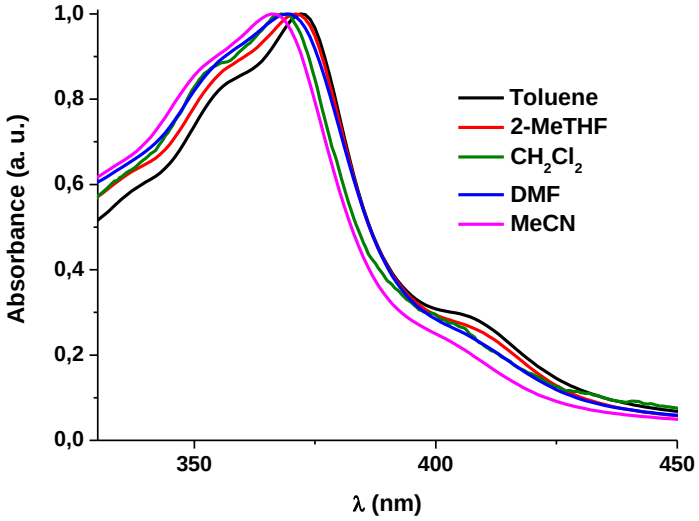


**Figure 7.** UV-Vis absorption spectra of **1** in different solvents ($10^{-5}$ M) at 298 K

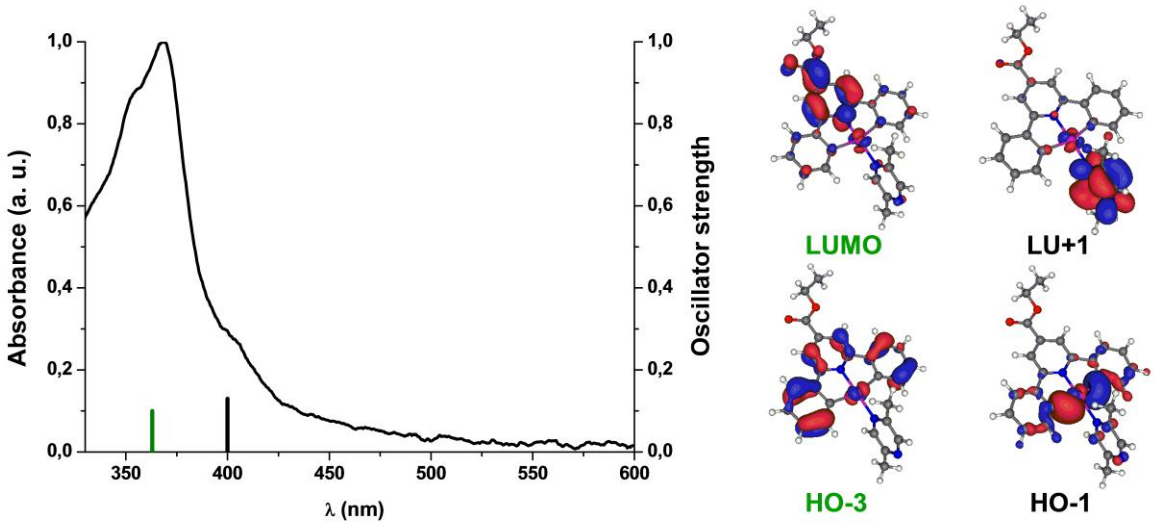


**Figure 8.** Left: calculated absorption spectra (bars) of **1** and experimental UV-Vis spectra in dichloromethane ($10^{-5}$ M) at 298 K. Right: Frontier orbital plots for **1** obtained by DFT

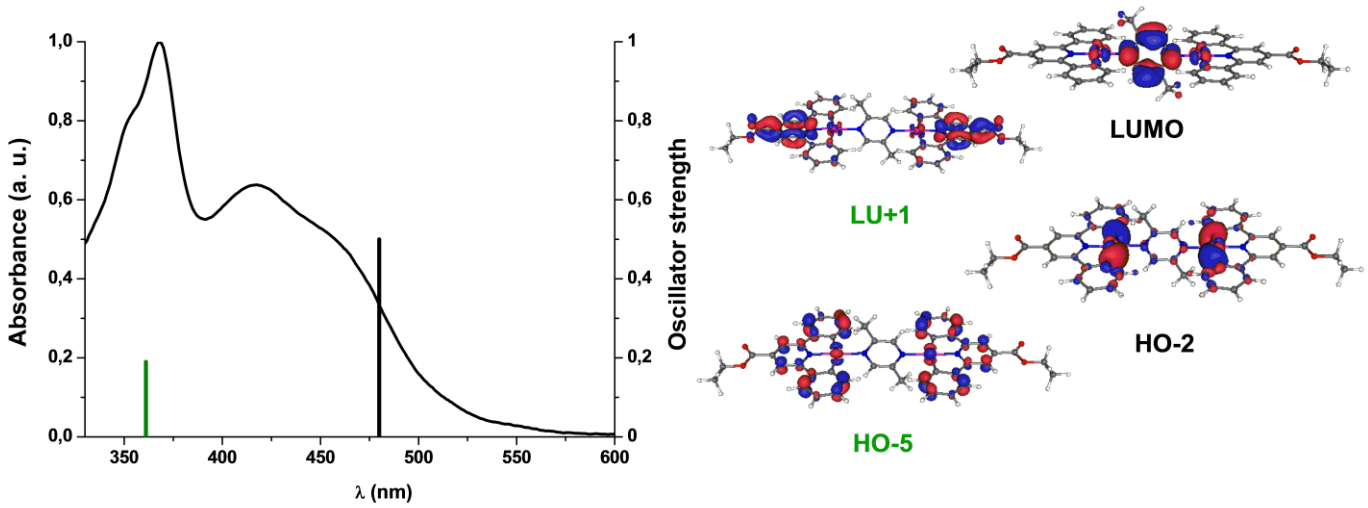


**Figure 9.** Left: calculated absorption spectra (bars) of **2** and experimental UV-Vis spectra in dichloromethane ($10^{-5}$ M) at 298 K. Right: Frontier orbital plots for **2** obtained by DFT

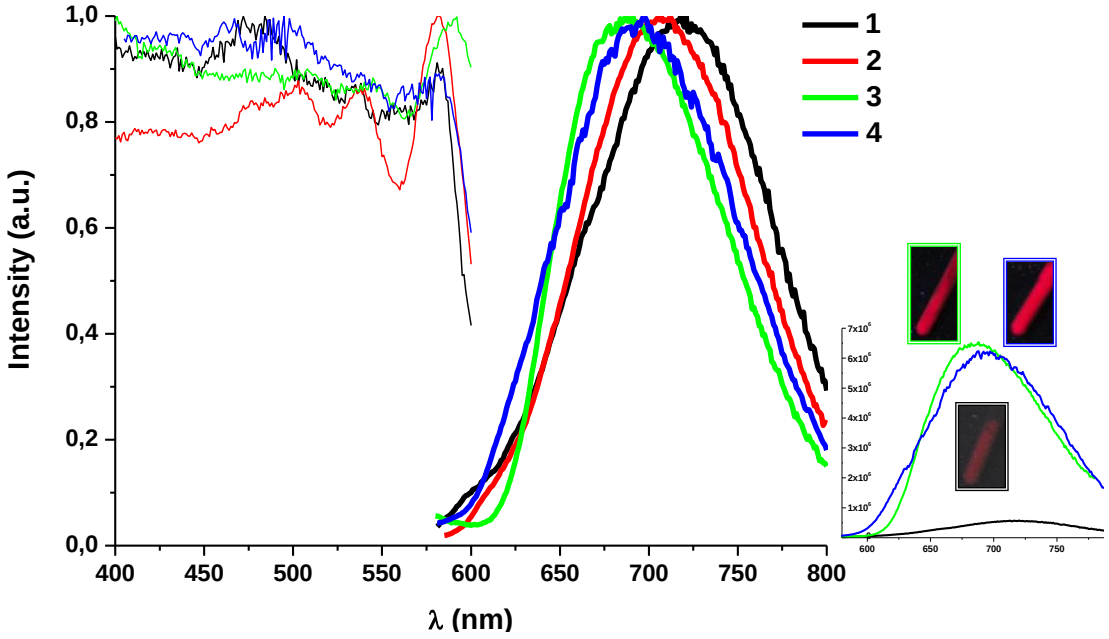


**Figure 10.** Normalized solid state excitation and emission spectra of **1**-**4** at 77 K. Inset: Pictures and not normalized emission spectra of **1**, **3** and **4**.

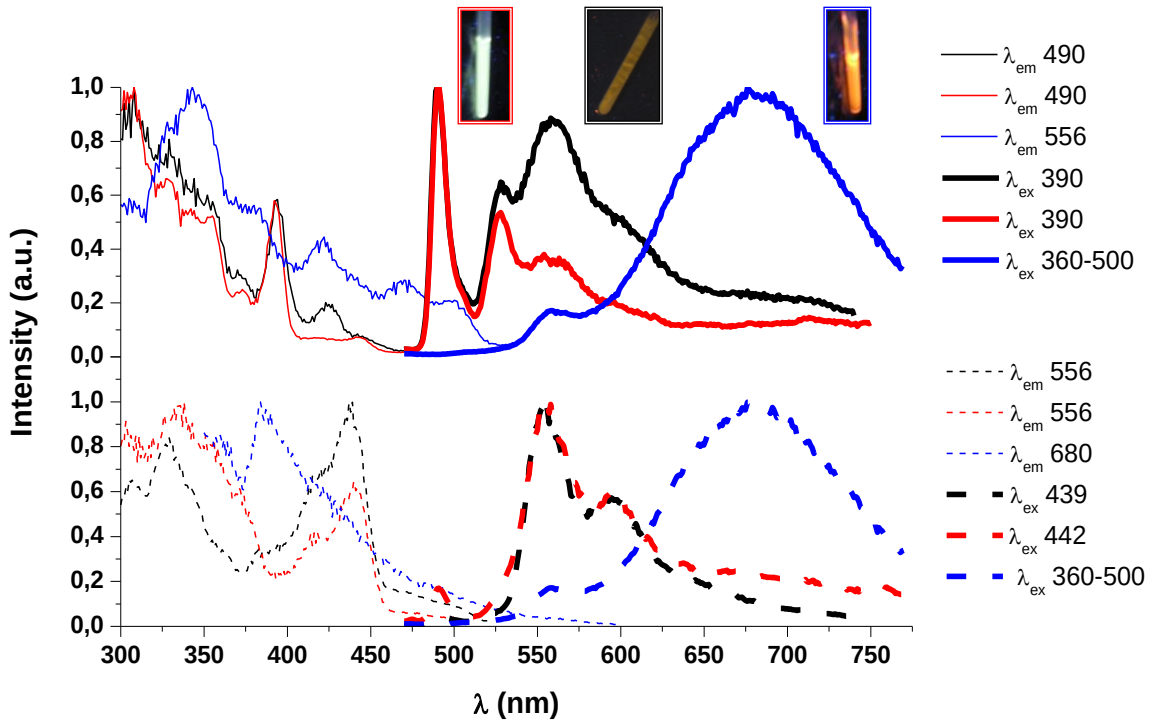


**Figure 11.** Normalized excitations and emission spectra of diluted glassy (5 x $10^{-5}$ M, 77 K) solutions of — **1**, — **2** and — **4** in 2-MeTHF, with λex <400 (top, solid line) and λex > 400 (bottom, dashed line). Pictures taken with a UV lamp (λex = 365 nm).

## References


1. Braunstein, P.; Oro, L. A.; Raithby, P. R.: In *Metal Clusters in Chemistry*; Wiley-VCH Verlag GmbH, 1999; Vol. Vol 3.
2. Adams, R. D.; Captain, B., *Accounts Chem. Res.* **2009**, *42*, 409-418.
3. Sivaramakrishna, A.; Clayton, H. S.; Makhubela, B. C. E.; Moss, J. R., *Coord Chem Rev* **2008**, *252*, 1460-1485.
4. Sculfort, S.; Braunstein, P., *Chem Soc Rev* **2011**, *40*, 2741-2760.
5. Adams, R. D.; Cotton, A. F.: Catalysis by Di- and Polynuclear Metal Cluster Complexes. Wiley-VCH: New York,, 1998; Vol. 14.
6. Lee, J.; Farha, O. K.; Roberts, J.; Scheidt, K. A.; Nguyen, S. T.; Hupp, J. T., *Chem Soc Rev* **2009**, *38*, 1450-1459.
7. Katz, M. J.; Sakai, K.; Leznoff, D. B., *Chem Soc Rev* **2008**, *37*, 1884-1895.
8. Qiu, S.; Zhu, G., *Coord Chem Rev* **2009**, *253*, 2891-2911.
9. Eddaoudi, M.; Moler, D. B.; Li, H. L.; Chen, B. L.; Reineke, T. M.; O'Keeffe, M.; Yaghi, O. M., *Accounts Chem. Res.* **2001**, *34*, 319-330.
10. Fornies, J.; Fuertes, S.; Martin, A.; Sicilia, V.; Lalinde, E.; Moreno, M. T., *Chem-Eur J* **2006**, *12*, 8253-8266.
11. Gil, B.; Forniés, J.; Gómez, J.; Lalinde, E.; Martín, A.; Moreno, M. T., *Inorg. Chem* **2006**, *45*, 7788-7798.
12. Wong, K. M. C.; Hui, C. K.; Yu, K. L.; Yam, V. W. W., *Coord Chem Rev* **2002**, *229*, 123-132.
13. Umakoshi, K.; Kojima, T.; Saito, K.; Akatsu, S.; Onishi, M.; Ishizaka, S.; Kitamura, N.; Nakao, Y.; Sakaki, S.; Ozawa, Y., *Inorg. Chem* **2008**, *47*, 5033-5035.
14. Moret, M. C.; Chen, P. J., *J. Am. Chem. Soc* **2009**, *131*, 5675-5690.
15. Yin, G.-Q.; Wei, Q.-H.; Zhang, L.-Y.; Chen, Z.-N., *Organometallics* **2006**, *25*, 580-587.
16. Lang, H.; del Villar, A.; Stein, T.; Zoufala, P.; Rueffer, T.; Rheinwald, G., *J. Organomet. Chem.* **2007**, *692*, 5203-5210.
17 Forniés, J.; Ibañez, S.; Martin, A.; Sanz, M.; Berenguer, J. R.; Lalinde, E.; Torroba, J., *Organometallics* **2006**, *25*, 4331-4340 and references therein.
18. Falvello, L. R.; Fornies, J.; Lalinde, E.; Menjon, B.; Garcia-Monforte, M. A.; Moreno, M. T.; Tomas, M., *Chem Commun* **2007**, 3838-3840.
19. Doerrer, L. H., *Comments on Inorganic Chemistry* **2008**, *29*, 93-127.
20. Doerrer, L. H., *Dalton Trans* **2010**, *39*, 3543-3553.
21. Balch, A. L.; Fung, E. Y.; Nagle, J. K.; Olmstead, M. M.; Rowley, S. P., *Inorg. Chem* **1993**, *32*, 3295-3299.
22. Casas, J. M.; Fornies, J.; Martin, A.; Orera, V. M.; Orpen, A. G.; Rueda, A. J., *Inorg. Chem* **1995**, *34*, 6514-6519.
23. Ruben Berenguer, J.; Diez, A.; Fernandez, J.; Fornies, J.; Garcia, A.; Gil, B.; Lalinde, E.; Moreno, M. T., *Inorg. Chem* **2008**, *47*, 7703-7716.
24. Ara, I.; Falvello, L. R.; Fornies, J.; Gomez-Cordon, J.; Lalinde, E.; Merino, R. I.; Uson, I., *J. Organomet. Chem.* **2002**, *663*, 284-288.
25. Yamaguchi, T.; Yamazaki, F.; Ito, T., *J. Am. Chem. Soc* **1999**, *121*, 7405-7406.
26. Fornies, J.; Ibanez, S.; Martin, A.; Gil, B.; Lalinde, E.; Moreno, M. T., *Organometallics* **2004**, *23*, 3963-3975.
27. Berenguer, J. R.; Gil, B.; Fernandez, J.; Fornies, J.; Lalinde, E., *Inorg. Chem* **2009**, *48*, 5250-5262.
28. Nagle, J. K.; Balch, A. L.; Olmstead, M. M., *J. Am. Chem. Soc* **1988**, *110*, 319-321.
29. Ara, I.; Berenguer, J. R.; Fornies, J.; Gomez, J.; Lalinde, E.; Merino, R. I., *Inorg. Chem* **1997**, *36*, 6461-6464.

30. Charmant, J. P. H.; Fornies, J.; Gomez, J.; Lalinde, E.; Merino, R. I.; Moreno, M. T.; Orpen, A. G., *Organometallics* **2003**, *22*, 652-656.
31. Fornies, J.; Fuertes, S.; Martin, A.; Sicilia, V.; Gil, B.; Lalinde, E., *Dalton Trans* **2009**, 2224-2234.
32. Diez, A.; Lalinde, E.; Teresa Moreno, M., *Coord Chem Rev* **2011**, *255*, 2426-2447.
33. Mealli, C.; Pichierri, F.; Randaccio, L.; Zangrando, E.; Krumm, M.; Holtenrich, D.; Lippert, B., *Inorg Chem* **1995**, *34*, 3418-3424.
34. Aullon, G.; Alvarez, S., *Inorg Chem* **1996**, *35*, 3137-3144.
35. Liu, J.; Sun, R. W.-Y.; Leung, C.-H.; Lok, C.-N.; Che, C.-M., *Chem Commun* **2012**, *48*, 230-232.
36. Liu, J.; Leung, C.-H.; Chow, A. L.-F.; Sun, R. W.-Y.; Yan, S.-C.; Che, C.-M., *Chem Commun* **2011**, *47*, 719-721.
37. Ma, D. L.; Che, C. M.; Yan, S. C., *J. Am. Chem. Soc* **2009**, *131*, 1835-1846.
38. Sun, R. W.-Y.; Chow, A. L.-F.; Li, X.-H.; Yan, J. J.; Chui, S. S.-Y.; Che, C.-M., *Chemical Science* **2011**, *2*, 728-736.
39. Wang, P.; Leung, C.-H.; Ma, D.-L.; Sun, R. W.-Y.; Yan, S.-C.; Chen, Q.-S.; Che, C.-M., *Angew. Chem.-Int. Edit.* **2011**, *50*, 2554-2558.
40. Ma, D. L.; Che, C. M., *Chem-Eur J* **2003**, *9*, 6133-6144.
41. Koo, C. K.; Wong, K. L.; Man, C. W. Y.; Lam, Y. W.; So, K. Y.; Tam, H. L.; Tsao, S. W.; Cheah, K. W.; Lau, K. C.; Yang, Y. Y.; Chen, J. C.; Lam, M. H. W., *Inorg Chem* **2009**, *48*, 872-878.
42. Wu, P.; Wong, E. L. M.; Ma, D. L.; Tong, G. S. M.; Ng, K. M.; Che, C. M., *Chem-Eur J* **2009**, *15*, 3652-3656.
43. Mou, X.; Wu, Y.; Liu, S.; Shi, M.; Liu, X.; Wang, C.; Sun, S.; Zhao, Q.; Zhou, X.; Huang, W., *Journal of Materials Chemistry* **2011**, *21*, 13951-13962.
44. Gareth Williams, J. A.; Develay, S.; Rochester, D. L.; Murphy, L., *Coord Chem Rev* **2008**, *252*, 2596-2611.
45. Murphy, L.; Williams, J. A. G.: Luminescent Platinum Compounds: From Molecules to OLEDs. In *Molecular Organometallic Materials for Optics*; LeBozec, H., Guerchais, V., Eds.; Springer-Verlag Berlin, 2010; pp 75-111.
46. Sotoyama, W.; Satoh, T.; Sawatari, N.; Inoue, H., *Appl. Phys. Lett.* **2005**, *86*.
47. Wong, W. Y., *J. Organomet. Chem.* **2009**, *694*, 2644-2647.
48. Zhou, G.; Wang, Q.; Wang, X.; Ho, C.-L.; Wong, W.-Y.; Ma, D.; Wang, L.; Lin, Z., *Journal of Materials Chemistry* **2010**, *20*, 7472-7484.
49. Rossi, E.; Murphy, L.; Brothwood, P. L.; Colombo, A.; Dragonetti, C.; Roberto, D.; Ugo, R.; Cocchi, M.; Williams, J. A. G., *Journal of Materials Chemistry* **2011**, *21*, 15501-15510.
50. Wong, W. Y.; Chow, W. C.; Cheung, K. Y.; Fung, M. K.; Djurisic, A. B.; Chan, W. K., *J. Organomet. Chem.* **2009**, *694*, 2717-2726.
51. Wong, W. Y.; Ho, C. L., *Accounts Chem. Res.* **2010**, *43*, 1246-1256.
52. Zhao, Q.; Li, F.; Huang, C., *Chemical Society Reviews* **2010**, *39*, 3007-3030.
53. Taylor, S. D.; Howard, W.; Kaval, N.; Hart, R.; Krause, J. A.; Connick, W. B., *Chem Commun* **2010**, *46*, 1070-1072.
54. Williams, J. A. G., *Top Curr Chem* **2007**, *281*, 205-268.
55. Balashev, K. P.; Puzyk, M. V.; Kotlyar, V. S.; Kulikova, M. V., *Coord Chem Rev* **1997**, *159*, 109-120.
56. Yam, V. W. W.; Chan, K. H. Y.; Wong, K. M. C.; Zhu, N. Y., *Chem-Eur J* **2005**, *11*, 4535-4543.
57. Fornies, J.; Fuertes, S.; Lopez, J. A.; Martin, A.; Sicilia, V., *Inorg Chem* **2008**, *47*, 7166-7176.

58. Diez, A.; Fornies, J.; Fuertes, S.; Lalinde, E.; Larraz, C.; Lopez, J. A.; Martin, A.; Moreno, M. T.; Sicilia, V., *Organometallics* **2009**, *28*, 1705-1718.
59. Lu, W.; Chan, M. C. W.; Cheung, K. K.; Che, C. M., *Organometallics* **2001**, *20*, 2477-2486.
60. Kui, S. C. F.; Chui, S. S. Y.; Che, C. M.; Zhu, N. Y., *J. Am. Chem. Soc* **2006**, *128*, 8297-8309.
61. Lai, S. W.; Lam, H. W.; Lu, W.; Cheung, K. K.; Che, C. M., *Organometallics* **2002**, *21*, 226-234.
62. Lu, W.; Mi, B. X.; Chan, M. C. W.; Hui, Z.; Che, C. M.; Zhu, N. Y.; Lee, S. T., *J. Am. Chem. Soc* **2004**, *126*, 4958-4971.
63. Fornies, J.; Garcia, A.; Lalinde, E.; Moreno, M. T., *Inorg Chem* **2008**, *47*, 3651-3660.
64. Berenguer, J. R.; Fernandez, J.; Gil, B.; Lalinde, E.; Sanchez, S., *Inorg Chem* **2010**, *49*, 4232-4244.
65. Diez, A.; Fernandez, J.; Lalinde, E.; Teresa Moreno, M.; Sanchez, S., *Inorg Chem* **2010**, *49*, 11606-11618.
66. Forniés, J.; Martin, A.: In *Metal Clusters in Chemistry*; Braunstein, P., Oro, L. A., Raithby, P. R., Eds.; Wiley-VCH Verlag GmbH, 1999; Vol. 1; pp 417-443 and references therein.
67. Falvello, L. R.; Fornies, J.; Garde, R.; Garcia, A.; Lalinde, E.; Moreno, M. T.; Steiner, A.; Tomas, M.; Uson, I., *Inorg Chem* **2006**, *45*, 2543-2552.
68. Yamaguchi, T.; Yamaguchizaki, F.; Ito, T., *J. Am. Chem. Soc* **2001**, *123*, 743-744.
69. Janzen, D. E.; Mehne, L. F.; VanDerveer, D. G.; Grant, G. J., *Inorg Chem* **2005**, *44*, 8182-8184.
70. Jamali, S.; Mazloomi, Z.; Nabavizadeh, S. M.; Milic, D.; Kia, R.; Rashidi, M., *Inorg Chem* **2010**, *49*, 2721-2726.
71. Fornies, J.; Sicilia, V.; Casas, J. M.; Martin, A.; Lopez, J. A.; Larraz, C.; Borja, P.; Ovejero, C., *Dalton Trans* **2011**, *40*, 2898-2912.
72. Tong, G. S. M.; Che, C. M., *Chem-Eur J* **2009**, *15*, 7225-7237.
73. Fuertes, S.; Brayshaw, S. K.; Raithby, P. R.; Schiffers, S.; Warren, M. R., *Organometallics* **2012**, *31*, 105-119.
74. Albinati, A.; Isaia, F.; Kaufmann, W.; Sorato, C.; Venanzi, L. M., *Inorg Chem* **1989**, *28*, 1112-1122.
75. Willermann, M.; Mulcahy, C.; Sigel, R. K. O.; Cerda, M. M.; Freisinger, E.; Miguel, P. J. S.; Roitzsch, M.; Lippert, B., *Inorg Chem* **2006**, *45*, 2093-2099.
76. Jude, H.; Bauer, J. A. K.; Connick, W. B., *Inorg Chem* **2005**, *44*, 1211-1220.
77. Berenguer, J. R.; Lalinde, E.; Torroba, J., *Inorg Chem* **2007**, *46*, 9919-9930.
78. Cave, G. W. V.; Alcock, N. W.; Rourke, J. P., *Organometallics* **1999**, *18*, 1801-1803.
79. Cave, G. W. V.; Fanizzi, F. P.; Deeth, R. J.; Errington, W.; Rourke, J. P., *Organometallics* **2000**, *19*, 1355-1364.
80. Kulikova, M. V.; Balashev, K. P.; Erzin, K., *Russ. J. Gen. Chem.* **2003**, *73*, 1839-1845.
81. Yam, V. W. W.; Tang, R. P. L.; Wong, K. M. C.; Lu, X. X.; Cheung, K. K.; Zhu, N. Y., *Chem-Eur J* **2002**, *8*, 4066-4076.
82. Roesky, H. W.; Andruh, M., *Coord Chem Rev* **2003**, *236*, 91-119.
83. Hunter, C. A., *Chem Soc Rev* **1994**, *23*, 101-109.
84. Desiraju, G. R., *Accounts Chem. Res.* **2002**, *35*, 565-573.
85. Arsenault, G. J.; Anderson, C. M.; Puddephatt, R. J., *Organometallics* **1988**, *7*, 2094-2097.
86. Falvello, L. R.; Fornies, J.; Martin, A.; Sicilia, V.; Villarroya, P., *Organometallics* **2002**, *21*, 4604-4610.

87. Uson, R.; Fornies, J.; Tomas, M.; Casas, J. M.; Cotton, F. A.; Falvello, L. R.; Llusar, R., *Organometallics* **1988**, *7*, 2279-2285.
88. Bondi, A., *Journal of Physical Chemistry* **1964**, *68*, 441-&.
89. Haftbaradaran, F.; Draper, N. D.; Leznoff, D. B.; Williams, V. E., *Dalton Trans* **2003**, 2105-2106.
90. Carlucci, L.; Ciani, G.; Proserpio, D. M.; Sironi, A., *J. Am. Chem. Soc* **1995**, *117*, 4562-4569.
91. Liu, H.-K.; Huang, X.; Lu, T.; Wang, X.; Sun, W.-Y.; Kang, B.-S., *Dalton Trans* **2008**, 3178-3188.
92. Bachman, R. E.; Andretta, D. F., *Inorg Chem* **1998**, *37*, 5657-5663.
93. Moret, M.-E.; Chen, P., *Organometallics* **2008**, *27*, 4903-4916.
94. Moret, M.-E.; Serra, D.; Bach, A.; Chen, P., *Angew. Chem.-Int. Edit* **2010**, *49*, 2873-2877.
95. Kubas, G. J., *Inorg. Synth.* **1990**, *28*, 68-70.